Title

Bulk phase resource ratio alters carbon steel corrosion rates and endogenously produced extracellular electron transfer mediators in a sulfate-reducing biofilm

Journal

Biofouling, 35(6)

ISSN

0892-7014

Authors

Krantz, Gregory P

Lucas, Kilean

Wunderlich, Erica L-

et al.

Publication Date

2019-07-03

DOI

10.1080/08927014.2019.1646731

Peer reviewed

Title: **Bulk phase resource ratio alters carbon steel corrosion rates and endogenously-produced extracellular electron transfer mediators in a sulfate-reducing biofilm**

Authors: Gregory P. Krantz[1,2], Kilean Lucas[3], Erica L. -Wunderlich[4], Linh T. Hoang[4], Recep Avci[3], Gary Siuzdak[4,5], Matthew W. Fields*[1,2,5]

Affiliations:
[1]Department of Microbiology and Immunology, Montana State University, Bozeman, MT, USA

[2]Center for Biofilm Engineering, Montana State University, Bozeman, MT USA

[3]Image and Chemical Analysis Laboratory, Montana State University, Bozeman, MT, USA

[4]Scripps Center for Metabolomics and Mass Spectrometry, The Scripps Research Institute, La Jolla, CA, USA

[5]ENIGMA (http://enigma.lbl.gov/)

Key words: biocorrosion; microbiologically-influenced corrosion; MIC; *Desulfovibrio*

Correspondence:
M.W. Fields, PhD
Director, Center for Biofilm Engineering
Professor, Department of Microbiology & Immunology
366 Barnard Hall
Montana State University
Bozeman, MT 59715
406-994-7340

Word Count:
Main Document = 6,381
References = 1,487
Figure Captions = 453

ABSTRACT

Desulfovibrio alaskensis G20 biofilms were cultivated on 316 steel, 1018 steel, or borosilicate glass under steady-state conditions in electron-acceptor limiting (EAL) and electron-donor limiting (EDL) conditions with lactate and sulfate in a defined medium. Increased corrosion was observed on 1018 steel under EDLconditions compared to 316 steel, and biofilms on 1018 carbon steel under the EDL condition had at least 2-fold higher corrosion rates compared to the EAL condition. Protecting the 1018 metal coupon from biofilm colonization significantly reduced corrosion, suggesting that the corrosion mechanism was enhanced through attachment between the material and the biofilm. Metabolomic mass spectrometry analyses demonstrated an increase in a flavin-like molecule under the 1018 EDL condition and sulfonates under the 1018 EAL condition. These data indicate the importance of S-cycling under the EAL condition and the EDL is associated to increased biocorrosion via indirect extracellular electron transfer mediated by endogenously produced flavin-like molecules.

INTRODUCTION

Microbiologically-influenced corrosion (MIC) is a widespread problem incurring significant financial cost to the petroleum industry, the country, and communities. Carbon steel oil pipelines can slowly corrode abiotically under a variety of conditions, and when sulfate-reducing communities are present, corrosion rates can be greatly accelerated (Whitney 1903, Enning et al. 2012, Enning and Garrelf 2014, and references therein). The cost of metal corrosion in the US alone is estimated to be 2% to 3% of GDP (Gross Domestic Product) (Enning and Garrelf 2014) and is particularly important to carbon steel energy pipeline infrastructure. Corrosion induced failures in infrastructure create hazards to health, safety, environment, and product

deliverability. Adding to scale of the problem, MIC occurs under a wide variety of environmental conditions, including marine, freshwater and terrestrial locations.

MIC can involve a variety of different microorganisms that include sulfate-reducing bacteria (SRB) and iron-reducing bacteria (IRB) (Little et al. 2007, Enning and Garrelfs 2014, Bonifay et al. 2017). Together with SRBs and IRBs, microbial consortia are typically involved in two mechanisms of MIC: EET-MIC (extracellular electron transfer, Type I), cross membrane electron transfer (indirect and/or direct) (Kato 2016 and references therein), and/or metabolite-MIC (Type II), biocorrosion caused by secreted metabolites (*e.g.*, H^+, organic acids, sulfides) as opposed to chemical corrosion which can refer to direct metal-oxidant interactions (Li et al. 2018, Kannan et al 2018). Both EET-MIC and M-MIC are electrochemical corrosion processes (Li et al. 2018, Dinh et al. 2004), and different EET mechanisms can promote the transfer of electrons to or from extracellular solid compounds (Gralnick and Newman 2007, Kato 2016). The process of EET can be mediated directly with metal surfaces via cellular connections and/or conductive extracellular structures (*e.g.*, Gorby et al. 2006) or indirectly via diffusible redox molecules (Watanabe et al. 2009). The goal of this study was to elucidate nutrient ratio impacts on potential M-MIC and/or EET-MIC mechanisms during initial biofilm formation under continuous growth conditions in a defined growth medium.

Extracellular electron transfer, which is shown to enhance MIC, is now recognized as a more widespread microbial phenotype and suggests that EET-MIC could be a major mechanism for biocorrosion world-wide (Nealson and Saffarini, 1994, Kato 2016, Huang et al. 2018). Previous work postulated that some SRBs contribute to MIC under various growth conditions through Fe^0 oxidation via interactions with carbon steel (Gu, 2012; Venzlaff et al. 2013; Enning and Garrelfs 2014, Li et al. 2015). In addition to heme redox centers of cytochromes, cell-secreted

molecules have been shown to serve as electron carriers in EET processes in both *Shewanella oneidensis* and *Geobacter sulfurreducens* (Marsili et al. 2008; Okamoto et al. 2014), and more recently, flavin mononucleotide (FMN) and riboflavin were proposed to function in a diffusion-based EET (2 e^-) or bifurcated direct EET (1 e^-) in *Shewanella* (Okamoto et al. 2014). Therefore, future work should focus to elucidate the physiological conditions under which EET mechanisms contribute to overall biocorrosion.

Carbon starvation was previously shown to be associated with more aggressive corrosion by *Desulfovibrio vulgaris* biofilms (Xu and Gu 2014, Chen et al. 2015) and demonstrated the prolonged survival of *D. vulgaris* biofilms in the absence of organic electron donors. Studies with *D. vulgaris* 7757 showed that the addition of flavin adenine dinucleotide (FAD) or riboflavin could accelerate corrosion of 304 stainless steel and 1018 carbon steel (Li et al. 2015; Zhang et al. 2015), and electron transfer was hypothesized to be a limiting step for biocorrosion by *D. vulgaris*. While a relationship between nutrient deprivation and continued/accelerated biocorrosion has been shown for *Desulfovibrio*, the mechanism (Type I or II) under the nutrient deprived state is not known. We recently demonstrated that nutrient ratios impacted metal interactions (*i.e.*, Cr(VI) sensitivity) in *Desulfovibrio* (Franco et al. 2018), and therefore, hypothesized that nutrient imbalance would impact reduction-oxidation reactions in *Desulfovibrio* biofilms grown on a metal surface.

In the presented study, the corrosion rates and biofilm growth parameters under specific limiting nutritional ratios (*i.e.*, electron donor:acceptor imbalance) were measured with chemostat biofilms under defined culture conditions (*i.e.*, without yeast extract). *Desulfovibrio alaskensis* G20, isolated from a producing oil well in Ventura, CA (Hauser et al. 2011), was grown as a biofilm on glass, 316 stainless steel, and 1018 carbon steel with lactate as electron donor and

sulfate as electron acceptor in a defined medium. Electron-acceptor (EAL) and electron-donor (EDL) limited growth was achieved by adjusting relative concentrations (EAL-50:15; EDL-15:15) in the chemostat medium. *Desulfovibrio* G20 demonstrated increased corrosion on 1018 carbon steel under the EDL condition, and biofilm attachment with the steel was required for maximal corrosion rates. Global metabolomic results show increased sulfolactate levels under the EAL condition, which may indicate recycling sulfonate compounds for use as electron acceptors when limited for sulfate. Additionally, increased lumichrome levels were observed under the EDL condition on 1018 carbon steel, and these results suggested *Desulfovibrio* G20 produced flavin molecules that could be used to mediate extracellular electron transfers from steel Fe^0.

MATERIALS AND METHODS

Microorganism. *Desulfovibrio alaskensis* G20 was grown in a defined (without yeast extract) lactate/sulfate (LS4D) medium prepared anoxically as previously described under a variety of conditions (see below). Modifications to the original recipe included adjusting the lactate and sulfate concentrations to 50 mM lactate:15 mM sulfate for EAL conditions and 15 mM lactate: 15 mM sulfate for EDL conditions. As previously described, the medium was not prepared with reducing agent (Clark et al. 2006), and the use of resazurin in the culture medium served as a general indicator of oxidative-reduction potential (ORP). Sodium hydrosulfite (18 μg l^{-1}) was added to the 10% resazurin solution to shift the solution from purple to pink.

Planktonic Growth. *D. alaskensis* G20 was cultivated in media with respective nutrient ratios at 37°C, 30°C and 20°C for initial planktonic cultures. The defined growth medium for both planktonic and biofilm growth was anoxically prepared and used as previously described (Clark et al. 2006, Clark et al. 2007, Klonowoska et al. 2008, Clark et al. 2012, DeLeon et al. 2017). All

N_2 gas (99.995% purity) was run through an oxygen-scrubber before being used to sparge any liquids or head-space as previously described at a rate of approximately 1 ml/min (Brileya et al. 2014, Franco et al. 2018). Each batch condition was grown in triplicate in a Balch tube with anoxic N_2 headspace and sealed with butyl stoppers and a crimp seal. Optical Density (600 nm) was measured with a UNICO 1100RS spectrophotometer (New Jersey) and compared with uninoculated medium.

Biofilm Growth. Biofilm samples were grown in CDC Biofilm Reactors (Biosurface Technologies Corp., Bozeman, MT) with the headspace sparged with anoxic N_2 gas (run through oxygen-scrubber). Separate reactors were used to cultivate G20 biofilms on each surface type: glass, 316 stainless steel, and 1018 carbon steel under each limiting nutrient condition. The 1018 and 316 carbon steel coupons were not polished and used as received from Biosurface Technologies Corp. (Bozeman, MT). Reactors were inoculated with 40 ml of an exponential-phase culture and allowed to grow in batch mode for approximately 24 h. The medium pump flow rate was set to 0.3 ml min^{-1} (~D= 0.05 h^{-1}) 24 h post-inoculation and maintained continuous flow until final samples were harvested. The dilution rate was chosen because the influent growth medium did not contain additional reducing agent as previously reported (Clark et al. 2006, Clark et al. 2012) and *in situ* growth rates are typically slower. The starting pH of medium was approximately 7.2 and during growth was 7.6 to 7.8. Glass coupon dimensions were 7.1 x 1.25 x 0.1 cm. Metal coupon dimensions were 7.6 x 1.5 x 0.1 cm. Modified coupon holders were used as previously described to provide increased material surface area (Clark et al. 2012).

Biofilm and Coupon Harvesting. Biofilm coupons were removed from the reactor and biofilm was immediately removed from the coupon using a sterile scraper. Biomass was scraped into 3 ml of dH_2O and homogenized by adding sand and vortexing prior to growth parameter

measurements. The scraped coupon was dried and then treated according to standard practice for cleaning and evaluating corrosion samples (ASTM G1-03) with Clark Solution (6M HCl, 3.5 g l^{-1} hexamethylenetetramine) for 0.5 min before washing in nanopore H_2O and dried with dry nitrogen gas as previously described (Avci et al., 2013). The coupons incubated in sterile, anoxic medium (EAL or EDL levels of lactate and sulfate) for the same time period displayed approximately 0.01±0.01 mm/y mass loss. The post-exposure coupon mass was subtracted from the pre-exposure mass to obtain the mass loss, and the value of mm y^{-1} or mg cm^{-2} was calculated as described in ASTM G1-03. Relative electrochemical measurements were made to the reference electrode in the presence of cells and compared between the EDL and EAL conditions.

Electrochemical measurements. Electrochemical measurements were conducted with a conventional three-electrode system. A 1018 carbon steel coupon was made into a working electrode by spot welding the stripped end of Teflon coated wire. The exposed wire was coated with epoxy for insulation. The counter electrode was a platinum wire. The working electrode (the corroding carbon steel coupon) was not disturbed and used multiple times very briefly (<1 min duration) for time dependent resistance measurements. An electrochemical polarization curve was run with the PAR273 between 20 mV and -20 mV with respect to the approximate open circuit potential of 610 mV, with intervals of 0.1 mV. Readings were taken every 200 ms.

A reference electrode was constructed because commercial probes were not the correct length for the reactor. A silver wire (0.25 mm or 0.5 mm) was cleaned with 600 grit sand paper to remove oxide coating, the bottom 2 cm of this wire (the end that forms the electrode tip) was submerged in 1M HNO_3 for a few seconds, then washed with nanopure water and dried with N_2 gas. The wire was setup in a potentiostatic experiment with a EG&G Princeton Applied Research 273 potentiostat/galvanostat (Advanced Measurement Technology, Oak Ridge, TN) was used as

suggested by the manufacturer without solution resistance compensation. It should also be noted that previous work using this method confirmed predicted corrosion via atomic force microscopy measurements (Martin, 2014). The silver wire was the working electrode, a graphite rod was the counter electrode, and a purchased standard Ag/AgCl electrode was used as the reference electrode. The lower 2 cm of the silver wire was submerged in 0.1M HCl, and 1 V was applied to create 0.05-0.1 mA of current for 3 h. A 3M KCl and 3% agar solution was prepared and heated. A glass capillary tube was inserted into the agar until the agar had risen 2 cm inside the tube. The coated silver wire was pushed down the capillary until 1 cm from the bottom and in the middle of the agar. The wire-capillary assembly was removed from the agar and left to cool. Excess agar was wiped away and cut off the end of the capillary with a razor blade. A 3M KCl solution was gently added above the agar with a fine pipette. This was done carefully so no air bubbles remained in the capillary tube. The top of the newly constructed reference electrode was sealed with epoxy.

Preparation of Samples for Imaging. Biofilm samples were fixed by treatment in Karmovsky's Fixative (3.2% w/v paraformaldehyde, 2.5% w/w glutaraldehyde, 0.05M sodium cocodylate) for 16 h. Samples were soaked 4x in dH_2O for 5 min to remove fixative. Ethanol (EtOH) dehydration involved 5 min in 25% EtOH, 5 min in 50% EtOH, 5 min in 75% EtOH, 15 min in 95% EtOH, and 2 x 45 min in 100% EtOH before storage in 100% EtOH. Dehydrated samples were dried in a Tousimis Samdri-795 Critical Point Dryer (Tousimis Research Corporation, Rockland MD) using liquid CO_2 and a 10 min purge time. Dried samples were coated with Iridium for 30 s with an Emitech K575X Sputter Coater. Electron microscopy samples were imaged with a Zeiss Supra 55VP Field Emission Scanning Electron Microscopy (FE-SEM) (Carl Zeiss, Oberkochen, Germany) equipped with energy dispersive x-ray analysis (EDX). Images were false-colorized using Pixelmator (Vilnius, Lithuania) and Adobe Photoshop (San Jose, CA).

Microscopy of Biofilm Cross Sections. Biofilm coupons were incubated in acridine orange solution (4 g l^{-1}) for 1.5 h before being coated with Optimal Cutting Temperature Compound (Fisher Health Care) and frozen on a block of dry ice. The frozen biofilm was removed from the metal coupon by bending the steel coupon and stored at -80°C. The frozen biofilm samples were cut in half and sectioned with a Leica CM1850 cryostat (-20°C) at 5 μm slices and applied to a microscope slide for imaging. Images were taken with a Nikon Eclipse E800 microscope (Nikon Corporation, Minato, Tokyo, Japan) with a Photometrics Coolsnap MYO camera (Photometrics, Tuscon, AR). Images were taken at a FITC (fluorescein isothiocyanate) emission wavelength and differential interference contrast and overlaid using Metamorph software package (Molecular Devices, Sunnyvale, CA).

Growth Parameter Measurements. Protein concentrations were measured with a Qubit Protein Assay Kit (Life Technologies, Carlsbad, CA). Carbohydrate concentration was measured as previously described (Clark et al., 2006). Lactate and acetate were quantified using an Ultimate 3000 High Performance Liquid Chromatography instrument with a 300 mm x 7.8 mm HPLC Organic Acid Analysis Aminex HPX-87H Ion Exclusion Column (Thermo Scientific, Dionex Germering, Germany). Sulfate and hydrogen sulfide concentrations were measured using a Hach Colorimeter (Hach, Co., Loveland, CO) with the associated sulfate assay (Method 10248) and sulfide assay (Method 8131).

Protected 1018 Steel Coupons. Round 1018 steel coupons (127 mm) were placed in Spectra/Por Standard RC dialysis membranes (Spectrum Labs, Rancho Dominguez, CA) with a 6-8 kD molecular weight cut-off during the reactor run. The clamped membranes with steel coupons inside were suspended in the growth medium of a CDC biofilm reactor, and growth parameters and inoculation was the same as for biofilm cultivation descried earlier.

Metabolomics and Data Processing. At 192 h, biofilm coupons (EAL and EDL on 1018 carbon steel) were dipped in degassed dH_2O and the biofilm biomass scraped into a sterile microcentrifuge tube with degassed dH_2O (4°C). The tubes were centrifuged at 10,000 rpm for 5 min at 4°C. The supernatant was removed and the cell pellet frozen with liquid N_2 and stored at -80°C. Samples were processed and data analyzed as previously described (Ivanisevic et al. 2013; Benton et al. 2015; Montenegro-Burke et al. 2016; Huan et al. 2017).

RESULTS and DISCUSSION

Planktonic growth under different resource ratios. Planktonic growth was impacted by temperature, and *D. desulfuricans* G20 grew the fastest at 37°C and the slowest at 20°C in defined medium with lactate and sulfate (60:50 ratio). The specific growth rates were 0.05 h^{-1}, 0.12 h^{-1}, and 0.19 h^{-1}, respectively for 20°, 30°, and 37°C, and the final yields were similar. *Desulfovibrio* G20 formed the thickest biofilm at 37°C based on protein content in biofilm samples (data not shown), which is closest to elevated temperatures of some oil pipelines. In addition, 37°C is the most commonly used temperature in the literature for *D. alaskensis* G20; therefore, all subsequent experiments were done at 37°C.

Growth rates were measured for planktonic cultures under the varied nutritional ratios that were tested in the described experiments. Maximum growth rates were similar at 0.21 h^{-1} for EAL, 0.19 h^{-1} for EDL, and 0.20 h^{-1} for the 60:50 condition. As expected, final yields (OD values) were higher in media that had increased lactate concentrations. The 60:50 condition had the highest final biomass yield due to increased lactate and sulfate concentrations. The 60:50 condition is the standard SRB media recipe used in numerous *Desulfovibrio* studies (Zhou et al. 2011) and was used as a basis for comparison in the described study. When planktonic biomass yields (protein)

were compared in terms of sulfate or acetate ($Y^{Sulfate}$ or $Y^{Acetate}$) consumed, the EAL and EDL conditions were similar (Table 1). When the conditions were compared based upon $Y^{Lactate}$, the EDL condition had a higher yield that was twice the $Y^{Lactate}$ for the EAL condition. However, in terms of $Y^{Acetate}$, the EAL condition was 1.5-fold higher compared to EDL and similar to the 60:50 condition. The planktonic culture results suggested that biomass generation from a given amount of electrogenic flow to sulfate was more efficient under the altered ratios for batch planktonic cells. The observations coincide with the theoretically low value of 0.06 mole of biomass ($C_5H_7O_2N$) produced per mole of lactate consumed (Eq 1) based upon assumed cellular stoichiometries for bacterial growth (McCarty 1971). The results suggest that planktonic cultures grown under the altered resource ratios (EAL and EDL) processed resource differently compared to the 60:50 condition in terms of lactate oxidized to acetate produced.

$$0.36\ SO_4^{2-} + 0.54\ H^+ + CH_3CHOHCOO^- + 0.06\ NH_3 + 0.11\ H_2O \rightarrow 0.18\ H_2S + 0.18HS^- + 0.72\ CO_2 + CH_3COO^- + 0.06\ C_5H_7O_2N \qquad \Delta G^{o'}=-88.96\ kJ/mol \qquad \text{Equation 1}$$

Biofilm on metal and glass. *Desulfovibrio* G20 formed and maintained visible biofilm on glass, 316 steel, and 1018 carbon steel within 48 h under the tested conditions of EDL and EAL growth conditions; and as expected, the 1018 carbon steel surface appeared to have visible biofilm form earlier. The FE-SEM images show the presence of biofilm cells and other material that is most likely a combination of cellular material and mineral precipitates (Figure 1). In addition, the biofilms on glass and 316 steel had lower cell density compared to the biofilms on 1018 steel (Figure 1), and this result corresponded to measured protein levels (Figure 2). As expected, the biofilm is visually less pronounced on the 316 steel surface, and biofilm/metal precipitates were easier to remove from the 316 steel compared to the 1018 steel under both EAL and EDL. The observed biofilms on 1018 steel were visually more complex and heterogeneous under both EDL

and EAL conditions. False-colored FE-SEM images showed a mixture of aggregated cells embedded within mineral precipitates for the EAL and EDL conditions (Figure 3a and b). Energy dispersive x-ray spectroscopy was used to differentiate materials based on elemental composition (data not shown), and the corrosion products (colored in orange) are abundant and likely composed of iron-sulfide minerals that have been previously shown to be conductive (Thauer 2007). The EDL biofilm displayed a combination of organic material that was most likely carbohydrate-based EPS and extracellular filaments in addition to cells. Filaments appeared similar to structures previously observed in *Desulfovibrio vulgaris* biofilms cultivated on glass under a nutrient ratio of 60:50 (Clark et al. 2006); however, the exact role of these structures is not known. However, *fla*G (gene DVU1442 annotated as a flagellin in *D. vulgaris* genome) was up-expressed in *D. vulgaris* biofilms (Clark et al. 2012); and a Δ*fla*G mutant was deficient in biofilm formation but not motility (unpublished data). Further work is needed to determine the exact role(s) of extracellular structures in SRB biofilms grown on different surfaces and conditions.

Biofilm biomass. Carbohydrate and protein were quantified every 48 h for glass, 316 steel, and 1018 steel surfaces for both EAL and EDL conditions. The two metal surfaces under both EAL and EDL conditions displayed increasing biofilm (both protein and carbohydrate) over the tested time course (192 h) with a trend of more biofilm under EAL conditions and the most biofilm overall on 1018 steel (Figure 2). Under EAL conditions, glass and 316 steel biofilms had higher carbohydrate to protein (C:P) ratios compared to 1018 steel, and the biofilms on all three surfaces increased carbohydrate levels from 144 to 192 h as the biofilm matured (Figure 2). Under EDL conditions, carbohydrate and protein levels remained low on the glass and 316 steel biofilms. For EDL 1018 steel biofilms at 192 h, the C:P ratio was higher (4.36) compared to the 1018 EAL 192 h biofilms (2.86). The C:P ratios were higher for 192 h glass and 316 steel EAL biofilms (4.0

and 6.0, respectively) than the 192 h glass and 316 steel EDL biofilms (1.5 and 1.2, respectively) (Figure 2). These results suggest that carbon allocation is altered in biofilms on different surfaces and nutrient ratios, namely carbohydrate allocation under EAL conditions and protein in EDL conditions. The location (intracellular v. extracellular) is unknown for the protein and carbohydrate allocation. The biofilm composition data suggests that the biofilms responded differently to different types of energy restriction and coincides with previous work that has shown *Desulfovibrio* biofilm has altered physiology (*i.e.*, electron-flow is altered) even when compared to sulfate-reducing planktonic cells (Clark et al. 2012).

Images were taken of the EAL and EDL biofilm cross-sections to measure biofilm thickness and show distribution of *Desulfovibrio* G20 cells. The EAL biofilm (~200μm) is approximately 4-fold thicker than the approximately ~50 μm EDL biofilm (Figure 4). The accumulation of corrosion products may aid in forming a textured surface to attach as well as an extracellular matrix to grow within; however, the accumulation of thicker biofilms under EAL conditions was not associated with increased corrosion. The availability of more carbon source likely contributed to thicker biofilm at the 192 h time point on glass and 316 steel under EAL conditions than compared to EDL conditions. The 1018 steel biofilms had higher hexose levels than protein under both EAL and EDL conditions. Previous research by Clark et al. (2006) showed protein to be the major component of *Desulfovibrio vulgaris* Hildenborough (DvH) biofilms, with carbohydrate levels being relatively low. Our current observations with glass and steel under EAL and EDL demonstrate that hexose levels can be altered in *Desulfovibrio* biofilms (up to 50% of biomass), and in several samples accounted for a majority of the biomass. Though DvH and G20 are both members of the *Desulfovibrio* genus, there are significant physiological differences between the two microorganisms. Under the EDL condition, there is significantly less protein and

hexose on the glass and 316 steel surfaces than on the 1018 steel. Though G20 is being fed the same levels of nutrients on all surfaces under the EDL condition, the protein levels were increased on 1018 compared to glass and 316.

Lactate/acetate levels. Lactate and acetate levels were measured from the biofilm reactors to assess growth physiology under biofilm reactor conditions (Figure S1, S2, and S3). Typically for *Desulfovibrio* species, lactate is converted to acetate in a 1:1 ratio (Eq.1). Because G20 consumes lactate and sulfate in a 2:1 ratio, the 15 mM of available sulfate allows G20 to oxidize 30 mM (of the 50 mM available in the EAL condition) lactate producing 30 mM of acetate. Measured levels of lactate and acetate were similar to predicted stoichiometries (Figure S1). Under the EAL condition (50 mM lactate: 15mM sulfate) *Desulfovibrio* G20 used slightly more than 30mM of the 50mM lactate available, corresponding to approximately 15mM lactate in the effluent for all three surface types. Theoretically, there should be 20mM lactate remaining under this condition and the missing carbon likely was used for biomass biosynthesis. The EAL acetate levels are approximately 30 mM at 50 h and remain near this level at the last time point (192 h).

Under the EDL condition, which contains 15 mM lactate: 15 mM sulfate, growth is limited by lactate, which is expected to be entirely consumed. Within 50 h, lactate is not detectable in the EDL reactors after inoculation and remains below detection during reactor operation. With all of the lactate being consumed, the EDL acetate levels are expected to be at 15mM. Acetate levels reached approximately 12 mM at 50 h and remained at this level during reactor operation, likely representing carbon incorporation into biomass (Figure S1).

Sulfate levels. Under the EAL condition (50:15), as expected, the sulfate levels approach 2 mM or lower at 50 h and remain almost non-detectable during reactor operation for all three surface types (Figure S2). According to the 2:1 ratio of lactate: sulfate consumption, the EDL

condition (which contains 15mM lactate:15mM sulfate) would theoretically have 7.5 mM sulfate remaining in the medium. The EDL reactors (all surface types) approached 4 to 6 mM during reactor operation (Figure S2). While the measured sulfate levels are close to theoretical, there could have been some additional sulfate reduction dependent upon the oxidation of biomass in the reactor system (or Fe^0 from the carbon steel).

Sulfide levels. *Desulfovibrio* G20 reduces sulfate to sulfide, and sulfide levels were measured for both the planktonic and biofilm fractions normalized to protein levels for a given volume (planktonic) or surface area (biofilm) (Figure S3). Within each nutritionally limiting condition, the three surface types had similar planktonic sulfide concentrations; however, greater variation was observed in the last time point for EAL samples. The EAL planktonic samples maintained approximately 1 to 2 μg μg^{-1} (sulfide/protein) for each surface type, and the EDL condition maintained approximately 0.5 μg μg^{-1} (sulfide/protein) for each surface type (Figure S3). The results indicate that aqueous phase sulfide levels are higher under EAL conditions compared to EDL conditions for all tested surface types, and from a metal interaction perspective, higher sulfide levels generally translate to increased corrosion rates of carbon steel (Dinh et al. 2004).

The concentration of sulfide differed in biofilms grown on different surfaces (Figure S3). Under both EAL and EDL conditions, sulfide levels were higher on 1018 than on 316 steel or glass. EDL biofilms on average had higher sulfide levels, especially on 1018 carbon steel, than EAL biofilms. Despite the fact there was a thinner biofilm on 1018 under the EDL condition (Figure 2), the G20 biofilm produced more sulfide per unit surface area than under the EAL condition. This result was unexpected because the planktonic sulfide was lower under EDL compared to the EAL condition and suggested altered physiological conditions under the different energy restriction conditions (*e.g.*, more sulfide associated with biofilm biomass).

Corrosion rates. Corrosion for 316 stainless steel was minimal while the 1018 carbon steel showed a general corrosion under the tested conditions and time (data not shown). Corrosion rates calculated from mass loss (ASTM G1-03) were higher for the 1018 carbon steel compared to the 316 stainless steel coupons under both EAL and EDL conditions and less biofilm (protein and carbohydrate) was maintained on the 316 over the tested time period. These results suggested that the anti-corrosive properties of 316 can impede the type of corrosion observed with 1018 steel under the EDL condition. After 8 days, the estimated corrosion rate was the highest for 1018 steel under the EDL condition (Figure 5). Despite the higher planktonic sulfide levels under EAL conditions and thinner biofilm under EDL (Figure 4 and S3), the highest corrosion rate was observed under the EDL condition on 1018 steel (Figure 5). The increased EDL corrosion was further confirmed by electrochemical measurements and differences in 1/R values between EAL and EDL conditions on 1018 carbon steel (~3x). Electrochemical measurements can quantify the instantaneous corrosion rate, and the initial spike in corrosion occurred when the reactor was inoculated and a passivation layer of FeS_2 had not yet formed, likely due to abiotic processes. The EDL condition on 1018 steel had elevated electrochemical corrosion rate, and increased corrosion has also been observed by Xu and Gu (2014) and Chen et al. (2015) when *Desulfovibrio* biofilms were starved for nutrients under batch conditions.

Biofilm contact. In order to evaluate the importance of biofilm formation and presence on the metal surface for corrosion, biofilm formation on the metal was prevented by incubating 1018 carbon steel coupons in sealed 6-8 kD molecular weight cutoff dialysis tubing suspended in a CDC biofilm reactor growing *Desulfovibrio* G20. In addition, the same reactor contained coupons not in dialysis tubing (normal) to allow direct biofilm colonization and planktonic cell growth in the bulk medium. Under the normal condition where biofilm can form directly on the

metal surface, EDL showed increased corrosion (mass loss) compared to EAL; however, under the protected condition corrosion was decreased for both EDL and EAL (Figure 6). Moreover, the reduction in corrosion was greater (~3-fold decline) for the protected metal under the EDL condition (Figure 6). The results demonstrated that SRB biofilm attachment to and biofilm formation on the 1018 carbon steel surface was needed for maximal corrosion rates.

Metabolomic analysis on biofilm

Having observed a difference in corrosion rate between EAL and EDL biofilms on 1018 carbon steel, the mechanism involved in the increased corrosion caused by EDL-grown *Desulfovibrio* G20 was unknown. Metabolomic mass spectrometry analyses combined with XCMS data processing (Smith et al. 2012) was done on biofilm scraped from 1018 carbon steel grown under EAL and EDL conditions. A total of 1,157 features were detected between EDL and EAL ($p<0.01$) (Figure 7). Based on significance values and MS/MS confirmation, three metabolites of interest displayed significant fold changes (10 to 20-fold) (Table 2).

Sulfur cycling. One of the confirmed dysregulated metabolites, sulfolactate, was increased 15.7-fold under EAL conditions on 1018 steel (Figure 7). Sulfolactate is a sulfonate compound related to the cysteine/methionine processing pathways in some microorganisms. A complete pathway from cysteine to sulfolactate is not predicted in the *Desulfovibrio* G20 genome whereas the genome is annotated to contain an aminotransferase that could convert cysteate to sulfopyruvate (E.C. 2.6.1.1; KEGG). However, the genome annotation does not contain an identified enzyme to catalyze the conversion of sulfopyruvate to sulfolactate. The commonly identified enzymes with this activity include sulfolactate dehydrogenase (R and S) and malate dehydrogenase and would provide additional electron acceptor (reduction of sulfopyruvate to sulfolactate) via recycling of cysteine through cysteate and could account for the elevated

sulfolactate levels that were detected under EAL conditions. The *Desulfovibrio* G20 genome is annotated to have a gene that encodes a protein with potential malate dehydrogenase activity (Dde1008, NAD^+-linked). Sequence comparisons and biochemical studies have recently expanded the functionality of previously annotated malate and lactate dehydrogenases to have other activities such as sulfolactate dehydrogenase (Muramatsu et al. 2005); however, the potential role of Dde1008 in conversion of sulfopyruvate to sulfolactate is unknown.

The source of sulfopyruvate may be from the degradation of sulfur-containing amino acids cysteine and methionine, taking advantage of normal amino acid recycling as a means for generating sulfite (an additional electron acceptor). Other members of the *Desulfovibrio* family have demonstrated growth capabilities on sulfonate compounds such as cysteate or isethionate, as is the case with *Desulfovibrio desulfuricans* IC1 (Lie et al. 1996). Cysteate is the product from cysteine degradation and can be converted to 3-sulfopyruvate by cysteine lyase. However, cysteine lyase has not been identified in the *Desulfovibrio* G20 genome via annotation. The *Desulfovibrio* G20 genome is annotated to have the gene for aspartate aminotransferase (EC 2.6.1.1) that can convert cysteate to 3-sulfopyruvate. To explore whether G20 was able to utilize cysteate, planktonic growth with cysteate alone or with lactate was tested at similar ratios. Significant growth with cysteate was not observed with the tested growth medium (data not shown), and these results suggest that *Desulfovibrio* G20 cannot utilize cysteate as a sole source of carbon and energy.

Under the EAL condition, another significant metabolite that was identified at increased levels with high confidence was a cysteine-S-sulfate-related molecule (Table 2). Given the complexity of S-cycling, particularly in sulfate-reducing bacteria, the exact role of this compound is not known. A cysteine-S-sulfate molecule could be involved in cycling any available

intracellular sulfate, but a known annotated pathway has not been identified in *Desulfovibrio* G20. The presented results demonstrate the importance of S-cycling in *Desulfovibrio* G20 under EAL conditions, and further work is needed to fully elucidate the turnover of methionine/cysteine in SRBs and the potential effect on growth when limited for sulfate.

Role of electron shuttles. Under the EDL condition with increased 1018 steel corrosion, the metabolite lumichrome was increased 10-fold compared to the EAL condition (Table 2; Figure 7). Lumichrome is a by-product of riboflavin biosynthesis, and riboflavin is a predicted intermediate for the biosynthesis of FAD and FMN in both *D. vulgaris* and *Desulfovibrio* G20 genomes (Figure 8). *Desulfovibrio* G20 has annotated genes for the biosynthesis of riboflavin to FMN and FAD but does not have an annotated gene for the riboflavinase that can catalyze the conversion of riboflavin to lumichrome and ribitol (Figure 8). However, photolysis has been shown to drive the formation of lumichrome from riboflavin (Treadwell and Metzler 1972; Birss et al. 1997), particularly in anoxic conditions even under normal laboratory lighting, and the current anoxic reactors were exposed to ambient light during growth and the samples were processed in the light. The solubility of riboflavin, FMN, and FAD in water (0.12 g l^{-1}, 92 g l^{-1}, and 50 g l^{-1}, respectively) is much higher than lumichrome (0.0048 g/L). In addition, lumichrome has been shown to be an inhibitor of flavin oxidoreductase in *Escherichia coli* (Fieschi et al. 1995), and a protein family (dodecins) with high preference for lumichrome has been suggested to play a role in "trapping" riboflavin photolytic degradation products (*i.e.*, lumichrome) (Grininger et al. 2006). While lumichrome could play an unknown role in biofilm physiology, it is more likely that lumichrome is a photolytic by-product from riboflavin that has been shown previously to impact metal corrosion in SRBs (Kato 2016, Chen et al. 2015). Based upon these data and given that

Desulfovibrio G20 does not have an annotated riboflavinase, the detected lumichrome is likely related to riboflavin or flavin family molecules (*i.e.*, FMN and/or FAD)

Moreover, two metabolic features with the likely identity of FAD were increased 2.8 and 3.6-fold under the EDL condition. The p-values for these were 0.2, and while not meeting the statistical cutoff of 0.01, the FAD-molecules likely have biological (and corrosion) significance. Recent work in *Shewanella oneidensis* has demonstrated a role for FMN and riboflavin in which one-electron and two-electron mechanisms can play extracellular electron transfer roles under different conditions (Brutinel and Gralnick 2012; Okamoto et al. 2013). Interestingly, recent research demonstrated that adding FAD or riboflavin to *Desulfovibrio vulgaris* cultures increased metal corrosion rates in batch (Kato 2016, Chen et al. 2015). Our data further extends the role for flavin co-factors in metal corrosion and demonstrates a physiological condition (*i.e.*, EDL) in which biofilm would produce elevated levels of these compounds under metal-corroding conditions.

When considering the EDL condition and increased corrosion, elemental Fe could serve as a source of electrons for the biofilm under EET-MIC. Our data further supports the hypothesis that endogenous flavin compounds (*i.e.*, riboflavin, FMN, and FAD) could serve the role of extracellular electron transfer mediators for biofilm grown on 1018 carbon steel. When considering riboflavin, a one-electron transfer (semiquinone flavin) from Fe^0 (E_m=-0.167 V; Ksenzhek and Petrova 1983) would provide a favorable $\Delta G^{0'}$ value (-52 kJ) and if the semiquinone was further reduced the $\Delta G^{0'}$ value of the subsequent reaction would be -34 kJ. For the $FMN/FMNH_2$ couple (E_0'=-0.21 V; Mayhew 1999), a two-electron transfer from Fe^0 would provide a favorable $\Delta G^{0'}$ value (-44 kJ). For the $FAD/FADH_2$ couple (E_0'=-0.3 V; Curley et al. 1991), a two-electron transfer from Fe^0 would provide a favorable $\Delta G^{0'}$ value (-27 kJ). Based

solely upon thermodynamic estimations under standard conditions, riboflavin would be the preferred molecule, and this corresponds to more corrosion previously observed with riboflavin compared to FAD with *D. vulgaris* on 1018 carbon steel (Li et al. 2015). The results indicate that *Desulfovibrio* G20 biofilms likely produced endogenous flavin-like molecules when grown under EDL conditions on a metal surface.

CONCLUSION

The presented results demonstrate that energy restriction (EAL v. EDL) greatly impacted biofilm growth and physiology of *Desulfovibrio* G20 biofilms grown on carbon steel. Less corrosion was observed on 316 stainless steel compared to 1018 carbon steel for both EAL and EDL condition; however, the EDL condition promoted more corrosion of 1018 steel despite a thinner biofilm with decreased aqueous sulfide levels compared to the EAL condition. However, despite being limited for electrons under the EDL condition, more biofilm-associated sulfide was observed and corrosion was increased. In addition, the increased corrosion was dependent upon biofilm interaction with the metal surface. These results suggested that the metal surface was serving as an additional electron source (*i.e.*, Fe^0). Untargeted metabolomics indicated that the EAL-grown biofilm on 1018 steel altered cysteine/methionine cycling while the EDL-grown biofilm had elevated levels of flavin-like compounds. The flavin molecules likely serve a role in extracellular electron transfer when interacting with the metal surface (Fe^0) in EET-MIC (Figure 9), and this was further supported by the need for biofilm to interface directly with the metal surface for elevated corrosion. The endogenously-produced flavin molecules likely play a role to harvest electrons from Fe^0 when limited for electron donor, allowing continued biofilm growth under nutrient-restricted conditions. In essence, when lactate was limiting, sulfate reduction was

coupled to Fe^0 oxidation at the steel surface, thus promoting increased carbon steel corrosion. The results also suggest that the EDL condition could be relevant to the common practice of seawater injection into reservoir formations for enhanced oil extraction. Seawater has an average sulfate level of 28 mM, nearly twice the concentration used in this study. In hydrocarbon environments carbon/electron sources can be limiting due to slower degradation rates and/or competition for resources. Thus, the introduction of increased sulfate levels could shift the nutrient ratio in the EDL direction, thereby promoting increased corrosion rates via EET-MIC. Further work is needed to better understand the impact of energy imbalance on sulfate-reducing communities in different environments and the outcome on carbon steel materials.

ACKNOWLEDGMENTS

This material by ENIGMA- Ecosystems and Networks Integrated with Genes and Molecular Assemblies (http://enigma.lbl.gov), a Scientific Focus Area Program at Lawrence Berkeley National Laboratory is based upon work supported by the U.S. Department of Energy, Office of Science, Office of Biological & Environmental Research under contract number DE-AC02-05CH11231.

REFERENCES

Avci R, Davis BH, Wolfenden ML, Beech IB, Lucas K, Paul D. 2013. Mechanism of MnS-mediated pit iniation and propoagation in carbon steel in an anaerobic sulfidogenic media. Corr Sci. 76:267-274

Benton HP, Ivanisevic J, Mahieu NG, Kurczy ME, Johnson CH, Franco L, Rinehart D, Valentine E, Gowda H, Ubhi BK, Tautenhahn R, Gieschen A, Fields MW, Patti GJ, Siuzdak G. 2015. Autonomous metabolomics for rapid metabolite identification in global profiling. Anal Chem. 87:884–891.

Birss VI, Guha-Thakurta S, McGarvey CE, Quach S, Vanýsek P. 1997. An electrochemical study of the photolysis of adsorbed flavins. J Electroanal Chem. 423:13–21.

Bonifay V, Wawrik B, Sunner J, Snodgrass EC, Aydin E, Duncan KE, Callaghan AV, Oldham A, Liengen T, Beech I. 2017. Metabolomic and metagenomic analysis of two crude oil production pipelines experiencing differential rates of corrosion. Front Microbiol. 8:99.

Brileya KA, Camilleri LB, Zane GM, Wall JD, Fields MW. 2014. Biofilm growth mode optimizes carrying capacity during product inhibition syntrophy. Frontiers Microbiol. 5:693

Brutinel ED, Gralnick JA. 2012. Shuttling happens: soluble flavin mediators of extracellular electron transfer in *Shewanella.* Appl Microbiol Biotechnol. 93:41–48.

Chen Y, Tang Q, Senko JM, Cheng G, Zhang Newby B-M, Castaneda H, Ju L-K. 2015. Long-term survival of *Desulfovibrio vulgaris* on carbon steel and associated pitting corrosion. Corr Sci. 90: 89-100.

Clark ME, Edelmann RE, Duley ML, Wall JD, Fields MW. 2007. Biofilm formation in

Desulfovibrio vulgaris Hildenborough is dependent upon protein filaments. Environ Microbiol. 9:2844–2854.

Clark ME, He Q, He Z, Huang KH, Alm EJ, Wan X-F, Hazen TC, Arkin AP, Wall JD, Zhou J-Z, Fields MW. 2006. Temporal transcriptomic analysis as *Desulfovibrio vulgaris* Hildenborough transitions into stationary phase during electron donor depletion. Appl Environ Microbiol. 72:5578–5588.

Clark ME, He Z, Redding AM, Joachimiak MP, Keasling JD, Zhou JZ, Arkin AP, Mukhopadhyay A, Fields MW. 2012. Transcriptomic and proteomic analyses of *Desulfovibrio vulgaris* biofilms: Carbon and energy flow contribute to the distinct biofilm growth state. BMC Genomics. 13:138.

Curley GP, Carr MC, Mayhew SG, Voordouw G. 1991. Redox and flavin-binding properties of recombinant flavodoxin from *Desulfovibrio vulgaris* (Hildenborough). Eur J Biochem. 202:1091–1100.

De Leon KB, Zane GM, Trotter V, Krantz G, Arkin AP, Butland G, Walian P, Fields MW, Wall JD. 2017. Unintended laboratory-driven evolution reveals genetic requirements for biofilm formation by *Desulfovibrio vulgaris* Hildenborough. mBio 8:e01696-17

Dinh HT, Kuever J, Mussmann M, Hassel AW, Stratmann M, Widdel F. 2004. Iron corrosion by novel anaerobic microorganisms. Nature. 427:829–832.

Enning D, Venzlaff H, Garrelfs J, Dinh HT, Meyer V, Mayrhofer K, Hassel AW, Stratmann M, Widdel F. 2012. Marine sulfate-reducing corrosion bacteria cause serious corrosion of iron under electroconductive biogenic mineral crust. Environ Microbiol. 14:1772-1787.

Enning D, Garrelfs J. 2014. Corrosion of iron by sulfate-reducing bacteria: new views of an old problem. Appl Environ Microbiol. 80:1226–1236.

Fieschi F, Nivière V, Frier C, Décout JL, Fontecave M. 1995. The mechanism and substrate specificity of the NADPH:flavin oxidoreductase from *Escherichia coli*. J Biol Chem. 270:30392–30400.

Franco LC, Steinbeisser S, Zane GM, Wall JD, and Fields MW. 2018. Cr(VI) reduction and physiological toxicity are impacted by resource ratio in *Desulfovibrio vulgaris*. *Appl. Microbiol. Biotechnol*. 102:2839-2850.

Gorby, YA, Yanina S, McLean JS, Rosso KM, Moyles D, Dohnolkova A, Beveridge TJ, Chang IS, Kim BH, Culley DE, Reed SB, Romine MF, Saffarini DA, Hill EA, Shi L, Elias DA, Kennedy DW, Pinchuck G, Watanabe K, Ishill S, Logan B, Nealson KH, Fredrickson JK. 2006. Electrically condutive bacterial nanowires produced by *Shewanella oneidensis* strain MR-1 and other microorganisms. Proc. Natl. Acad. Sci *USA* 103:11358-11363.

Gralnick JA, Newman, DK. 2007. Extracellular respiration. Mol Microbiol. 65: 1–11.

Grininger M, Zeth K, Oesterhelt D. 2006. Dodecins: a family of lumichrome binding proteins. J Mol Biol. 357:842–857.

Gu T. 2012. New understandings of biocorrosion mechanisms and their classifications. J Microbial Biochem Technol. 4: iii-vi.

Hauser LJ, Land ML, Brown SD, Larimer F, Keller KL, Rapp-Giles BJ, Price MN, Lin M, Bruce DC, Detter JC, et al. 2011. Complete genome sequence and updated annotation of *Desulfovibrio alaskensis* G20. J Bacteriol. 193:4268–4269.

Huan T, Forsberg EM, Rinehart D, Johnson CH, Ivanisevic J, Paul Benton H, Fang M, Aisporna A, Hilmers B, Poole FL, Thorgersen MP, Adams MWW, Krantz G, Fields MW, Robbins PD, Niedernhofer LJ, Ideker T, Majumder EL, Wall JD, Rattray NJW, Goodacre R, Lairson LL, Siuzdak G. 2017. Systems biology guided by XCMS online metabolomics. Nat Methods. 14:461–462.

Huang Y, Zhou E, Jiang C, Jia R, Liu S, Xu D, Gu T, Wang F. 2018. Endogenous phenazine-1-carboxamide encoding gene *phz*h regulated the extracellular electron transfer in biocorrosion of stainless steel by marine *Pseudomonas aeruginosa*. Electrochem. Comm. 94:9-13.

Ivanisevic J, Zhu Z-J, Plate L, Tautenhahn R, Chen S, O'Brien PJ, Johnson CH, Marletta MA, Patti GJ, Siuzdak G. 2013. Toward omic-scale metabolite profiling: A dual separation–mass

spectrometry approach for coverage of lipid and central carbon metabolism. Anal Chem. 85:6876–6884.

Kannan P, Su SS, Mannan MS, Castaneda H, Vaddiraju S. 2018. A review of characterization and quantification tools for the microbiologically influenced corrosion in the oil and gass industry: current and future trends. Indust Eng Chem Res. 57:13895-13922.

Kato S. 2016. Microbial extracellular electron transfer and its relevance to iron corrosion. Microb Biotechnol. 9:141–148.

Klonowska A, Clark ME, Thieman SB, Giles BJ, Wall JD, Fields MW. 2008. Hexavalent chromium reduction in *Desulfovibrio vulgaris* Hildenborough causes transitory inhibition of sulfate reduction and cell growth. Appl Microbiol Biotechnol. 78:1007–1016.

Ksenzhek OS, Petrova SA. 1983. Electrochemical properties of flavins in aqueous solutions. J Electroanal Chem Interfacial Electrochem. 156:105–127.

Li H, Xu D, Li Y, Feng H, Liu Z, Li X, Gu T, Yang K. 2015. Extracellular electron transfer is a bottleneck in the microbiologically influenced corrosion of C1018 carbon steel by the biofilm of sulfate-reducing bacterium *Desulfovibrio vulgaris*. PLoS One. 10:e0136183.

Li Y, Xu D, Chen C, Li X, Jia R, Zhnag D, Sand W, Wang F, Gu T. 2018. Anaerobic microbiologically influenced corrosion mechanisms interpreted using bioenergetics and

bioelectrochemistry: A review. J Mat Sci Technol. 34:1713-1718.

Little BJ, Lee JS. 2007. Microbiologically Influenced Corrosion. John Wiley & Sons.

Malinauskas A, Ruzgas T, Gorton L. 1999. Tuning the redox potential of riboflavin by zirconium phosphate in carbon paste electrodes. Bioelectrochem Bioenerg. 49:21–27.

Martin J. 2014. Biocorrosion of 1018 steel in sulfide rich marine environments - a correlation between strain and corrosion using electron backscatter diffraction, Thesis, Montana State University.

Mayhew SG. 1999. The effects of pH and semiquinone formation on the oxidation--reduction potentials of flavin mononucleotide: a reappraisal. Eur J Biochem. 265:698–702.

McCarty PL. 1971. Energetics and bacterial growth. *In* SD Editors & JV Hunter (Eds), Organic compounds in aquatic environments p. 157–172, Faust New York: Marcel Dekker, Inc.

Montenegro-Burke JR, Phommavongsay T, Aisporna AE, Huan T, Rinehart D, Forsberg E, Poole FL, Thorgersen MP, Adams MWW, Krantz G, Fields MW, Northen TR, Robbins PD, Niedernhofer LJ, Lairson LL, Benton HP, Siuzdak G. 2016. Smartphone analytics: Mobilizing the lab into the cloud for omic-scale analyses. Anal Chem. 88: 9753–9758.

Muramatsu H, Mihara H, Goto M, Miyahara I, Hirotsu K, Kurihara T, Esaki N. 2005. A new

family of NAD(P)H-dependent oxidoreductases distinct from conventional Rossmann-fold proteins. J Biosci Bioeng. 99:541–547.

Nealson KH, Saffarini D. 1994. Iron and manganese in anaerobic respiration: environmental significance, physiology, and regulation. Annu Rev Microbiol. 48:311–343.

Okamoto A, Hashimoto K, Nealson KH, Nakamura R. 2013. Rate enhancement of bacterial extracellular electron transport involves bound flavin semiquinones. Proc Natl Acad Sci USA. 110:7856–7861.

Smith CA, Want EJ, O'Maille G, Abagyan R, Siuzdak G. 2006. XCMS: Processing mass spectrometry data for metabolite profiling using nonlinear peak alignment, matching, and identification. Anal Chem. 78:779–787.

Thauer RK, Stackebrandt E, Hamilton WA. 2007. Energy metabolism and phylogenetic diversity of sulphate-reducing bacteria. *In* Sulphate-reducing bacteria: Environmental and engineered systems (Eds. LJ Barton WA Hamilton), Chapter 1, 1–37.

Treadwell GE, Metzler DE. 1972. Photoconversion of riboflavin to lumichrome in plant tissues. Plant Physiol. 49:991–993.

Venzlaff H, Enning D, Srinivasan J, Mayrhofer KJJ, Hassel AW, Widdel F, Stratmann M. 2013.

Accelerated cathodic reaction in microbial corrosion of iron due to direct electron uptake by sulfate-reducing bacteria. Corr Sci. 66:88–96.

Watanabe K, Manefield M, Lee M, Kouzuma, A. 2009. Electron shuttles in biotechnology. Curr Opin Biotechnol. 20: 633–641.

Whitney WR 1903. The corrosion of iron. J Amer Chem Soc. 25:394-406.

Xu D, Gu T. 2014. Carbon source starvation triggered more aggressive corrosion against carbon steel by the *Desulfovibrio vulgaris* biofilm. Int Biodeterior Biodegradation. 91:74–81.

Zhang P, Xu D, Li Y, Yang K, Gu T. 2015. Electron mediators accelerate the microbiologically influenced corrosion of 304 stainless steel by the *Desulfovibrio vulgaris* biofilm. Bioelectrochemistry. 101:14–21.

Zhou J, He Q, Hemme CL, Mukhopadhyay A, Hillesland K, Zhou A, He Z, Van Nostrand JD, Hazen TC, Stahl DA, et al. 2011. How sulphate-reducing microorganisms cope with stress: lessons from systems biology. Nat Rev Microbiol. 9:452–466.

Figure Legends

Figure 1. Field Emission Scanning Electron Microscopy images were taken at 15,000X magnification for each condition (EAL and EDL) on glass, 316 stainless steel, and 1018 carbon steel.

Figure 2. (**a**) Hexose and protein levels on glass, 316 stainless steel, and 1018 carbon steel coupons under EAL conditions. (**b**) Hexose and protein on glass, 316 stainless steel, and 1018 carbon steel coupons under EDL conditions.

Figure 3. False colored Field Emission-Scanning Electron Microscopy image for (**a**) EAL and (**b**) EDL conditions. The colorized structures correspond to: Purple: G20 cells, Gold: iron sulfides, Blue: carbon-containing EPS, Green: extracellular filaments. The cells in the EAL condition are encrusted with iron-sulfide minerals.

Figure 4. Confocal images of thin-sectioned biofilms grown on 1018 carbon steel under (**a**) EAL and (**b**) EDL conditions. Biofilm ranges from 116-220 μm in thickness under EAL condition (**a**) to 50 μm under EDL condition (**b**). G20 cells are stained green. Substratum (carbon steel surface) is on the right.

Figure 5a. Corrosion rate (mm y^{-1}) for 316 stainless steel and 1018 carbon steel coupons during exposure to biofilm growth under EDL and EAL conditions.

Figure 5b. Corrosion rate (mg cm^{-2}) for 316 stainless steel and 1018 carbon steel coupons during exposure to biofilm growth under EDL and EAL conditions.

Figure 6. Corrosion rate of 1018 carbon steel coupons under normal exposure to *Desulfovibrio* G20 culture compared to coupons protected inside of dialysis tubing submerged in culture.

Figure 7. (**a**) Cloud plot of dys-regulated features comparing EAL versus EDL condition on 1018 carbon steel. All features shown have a P-value <0.01. (**b**) Intensities of sulfolactate peaks shown in EAL versus EDL. Lumichrome is increased 10.1-fold under EDL condition where increased corrosion rate is observed. (**c**) Sulfolactate is increased 15.7 fold under EAL condition.

Figure 8. Predicted riboflavin biosynthesis pathway in *Desulfovibrio* G20 and *D. vulgaris* based on KEGG predictions.

Figure 9. Classic model of corrosion with the addition of cycling endogenously produced flavin-based extracellular electron transfer molecules (Fm) with elemental Fe^0 within the biofilm as a form of EET (extracellular electron transfer)-MIC. The dashed arrow to H_2 could occur when electron acceptors (*e.g.*, sulfates) are at low levels.

Figure S1. (a) Lactate levels are shown under EAL condition on glass, 316 stainless steel, and 1018 carbon steel surfaces; as well as (b) Lactate levels under EDL condition on all three surface types. (c) Acetate levels under EAL condition on all 3 surfaces are shown with (d) Acetate levels under EDL condition on all three surface types.

740

741 **Figure S2**. (a) Planktonic sulfate concentrations under EAL conditions. (b) Planktonic sulfate
742 concentrations under EDL conditions.

743

744 **Figure S3**. Sulfide was measured and normalized to protein levels. Biofilm sulfide levels were
745 also normalized to surface area. (a) Planktonic sulfide concentrations under EAL conditions. (b)
746 Planktonic sulfide levels under EDL conditions. (c) Biofilm sulfide levels under EAL conditions.
747 (d) Biofilm sulfide levels under EDL conditions.

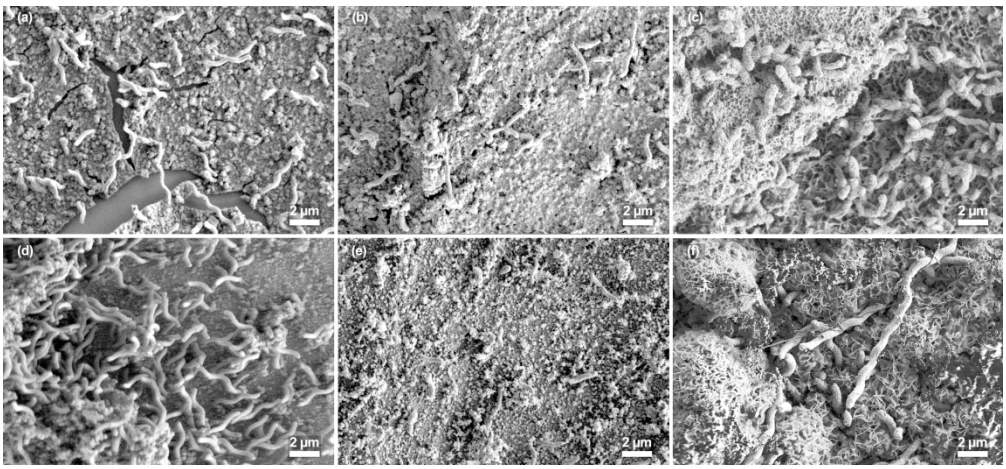

Figure 1. Field Emission Scanning Electron Microscopy images were taken at 15,000X magnification for each condition (EAL and EDL) on glass, 316 stainless steel, and 1018 carbon steel.

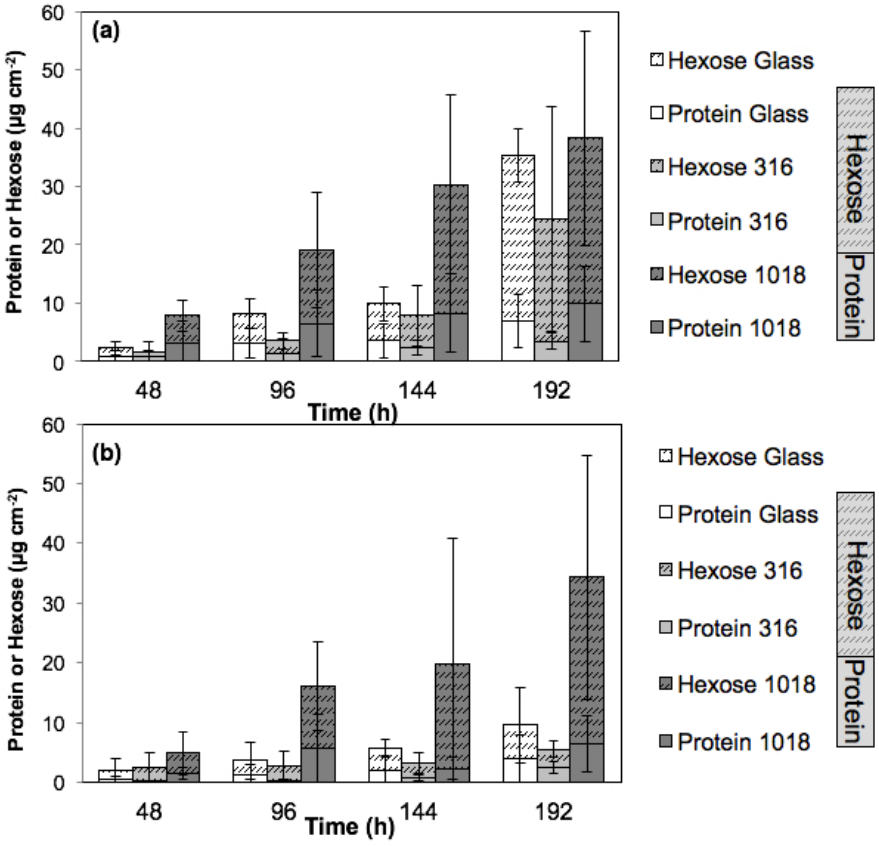

Figure 2. (a) Hexose and protein levels on glass, 316 stainless steel, and 1018 carbon steel coupons under EAL conditions. (b) Hexose and protein on glass, 316 stainless steel, and 1018 carbon steel coupons under EDL conditions.

238x211mm (72 x 72 DPI)

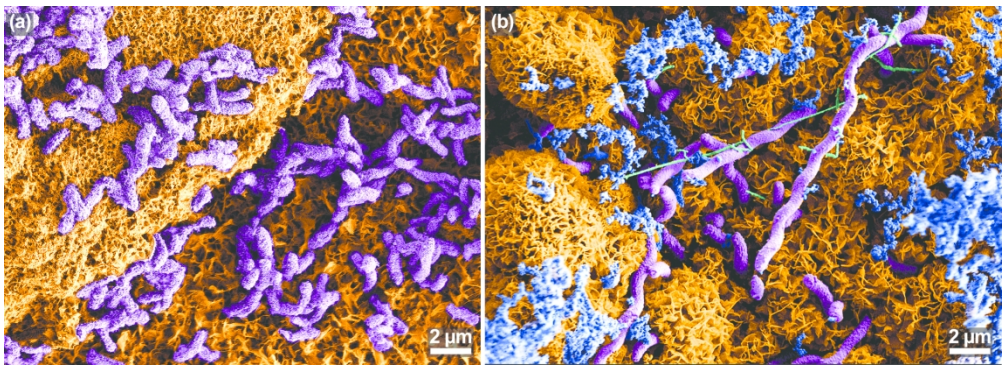

Figure 3. False colored Field Emission-Scanning Electron Microscopy image for (a) EAL and (b) EDL conditions. The colorized structures correspond to: Purple: G20 cells, Gold: iron sulfides, Blue: carbon-containing EPS, Green: extracellular filaments. The cells in the EAL condition are encrusted with iron-sulfide minerals.

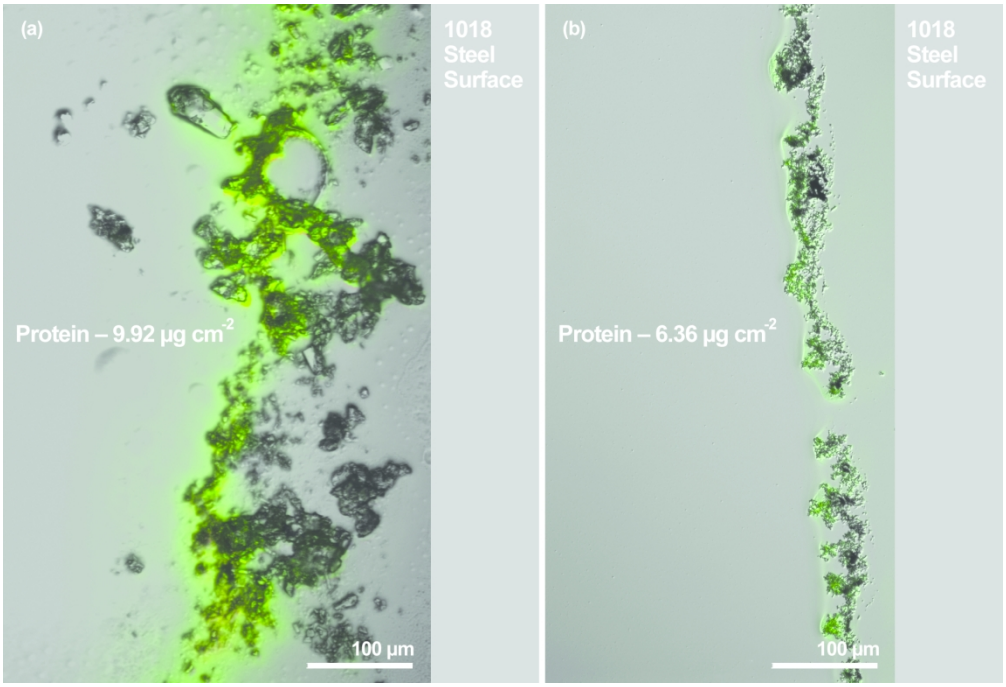

Figure 4. Confocal images of thin-sectioned biofilms grown on 1018 carbon steel under (a) EAL and (b) EDL conditions. Biofilm ranges from 116-220 µm in thickness under EAL condition (a) to 50 µm under EDL condition (b). G20 cells are stained green. Substratum (carbon steel surface) is on the right.

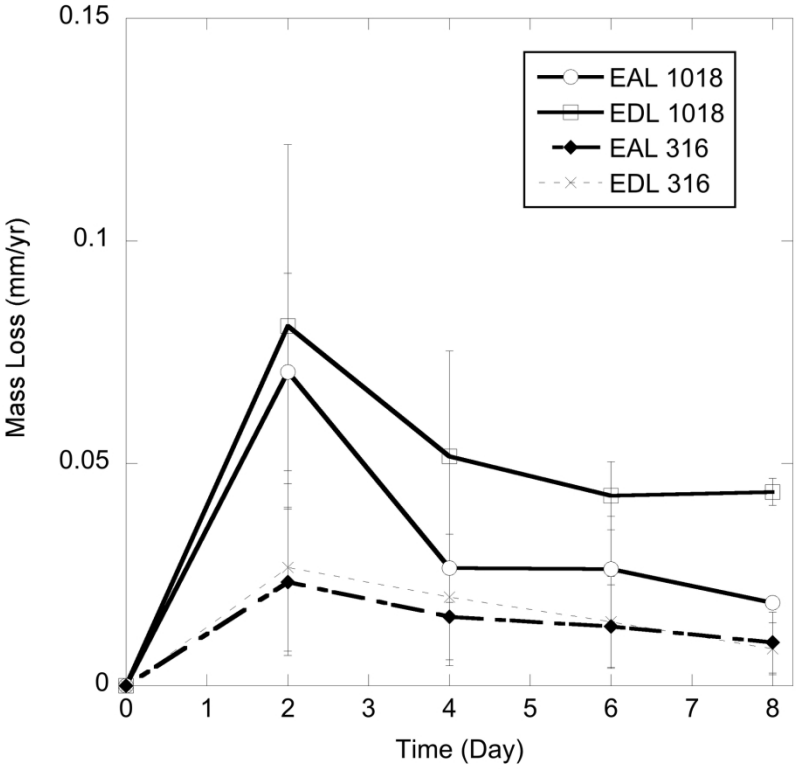

Figure 5a. Corrosion rate (mm y-1) for 316 stainless steel and 1018 carbon steel coupons during exposure to biofilm growth under EDL and EAL conditions.

190x190mm (300 x 300 DPI)

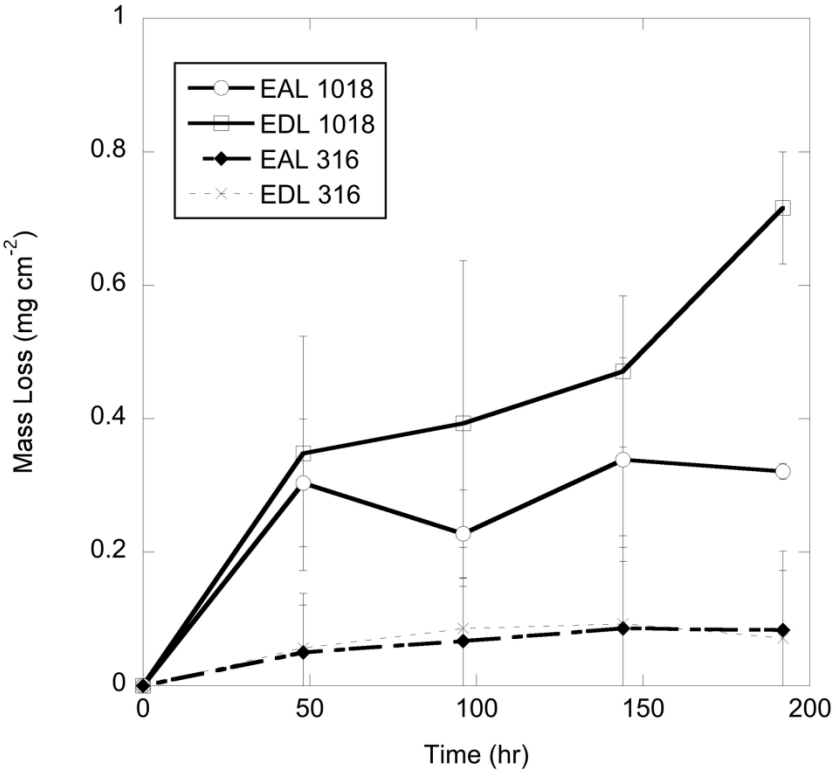

Figure 5b. Corrosion rate (mg cm-2) for 316 stainless steel and 1018 carbon steel coupons during exposure to biofilm growth under EDL and EAL conditions.

190x190mm (300 x 300 DPI)

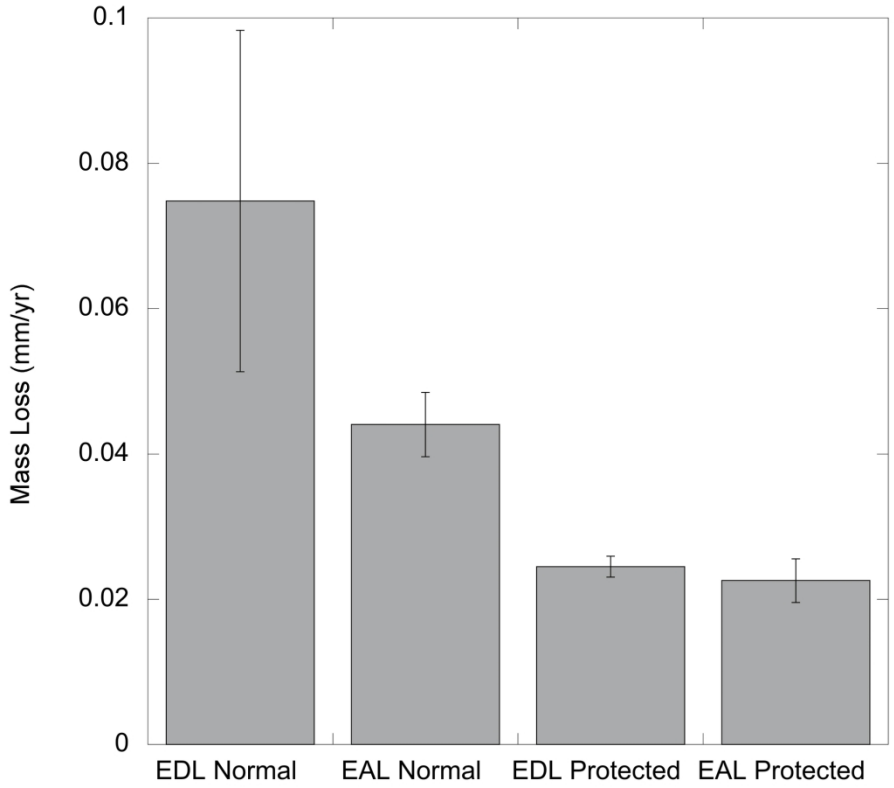

Figure 6. Corrosion rate of 1018 carbon steel coupons under normal exposure to Desulfovibrio G20 culture compared to coupons protected inside of dialysis tubing submerged in culture.

190x190mm (300 x 300 DPI)

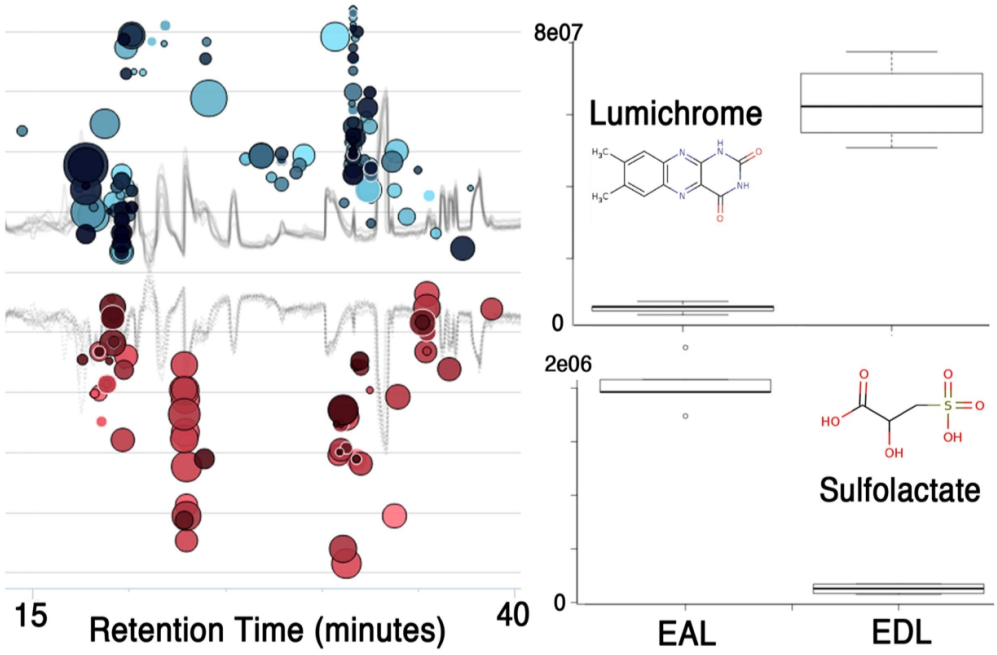

Figure 7. (a) Cloud plot of dys-regulated features comparing EAL versus EDL condition on 1018 carbon steel. All features shown have a P-value <0.01. (b) Intensities of sulfolactate peaks shown in EAL versus EDL. Lumichrome is increased 10.1-fold under EDL condition where increased corrosion rate is observed. (c) Sulfolactate is increased 15.7 fold under EAL condition.

103x68mm (300 x 300 DPI)

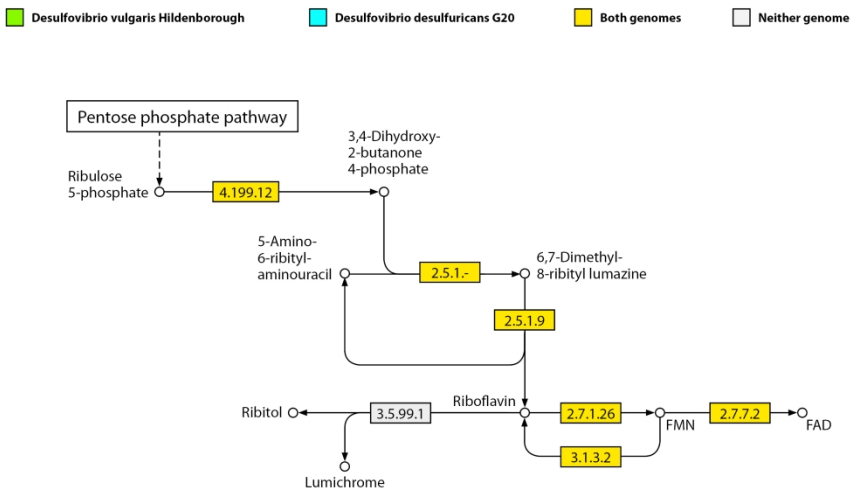

Figure 8. Predicted riboflavin biosynthesis pathway in Desulfovibrio G20 and D. vulgaris based on KEGG predictions.

279x215mm (300 x 300 DPI)

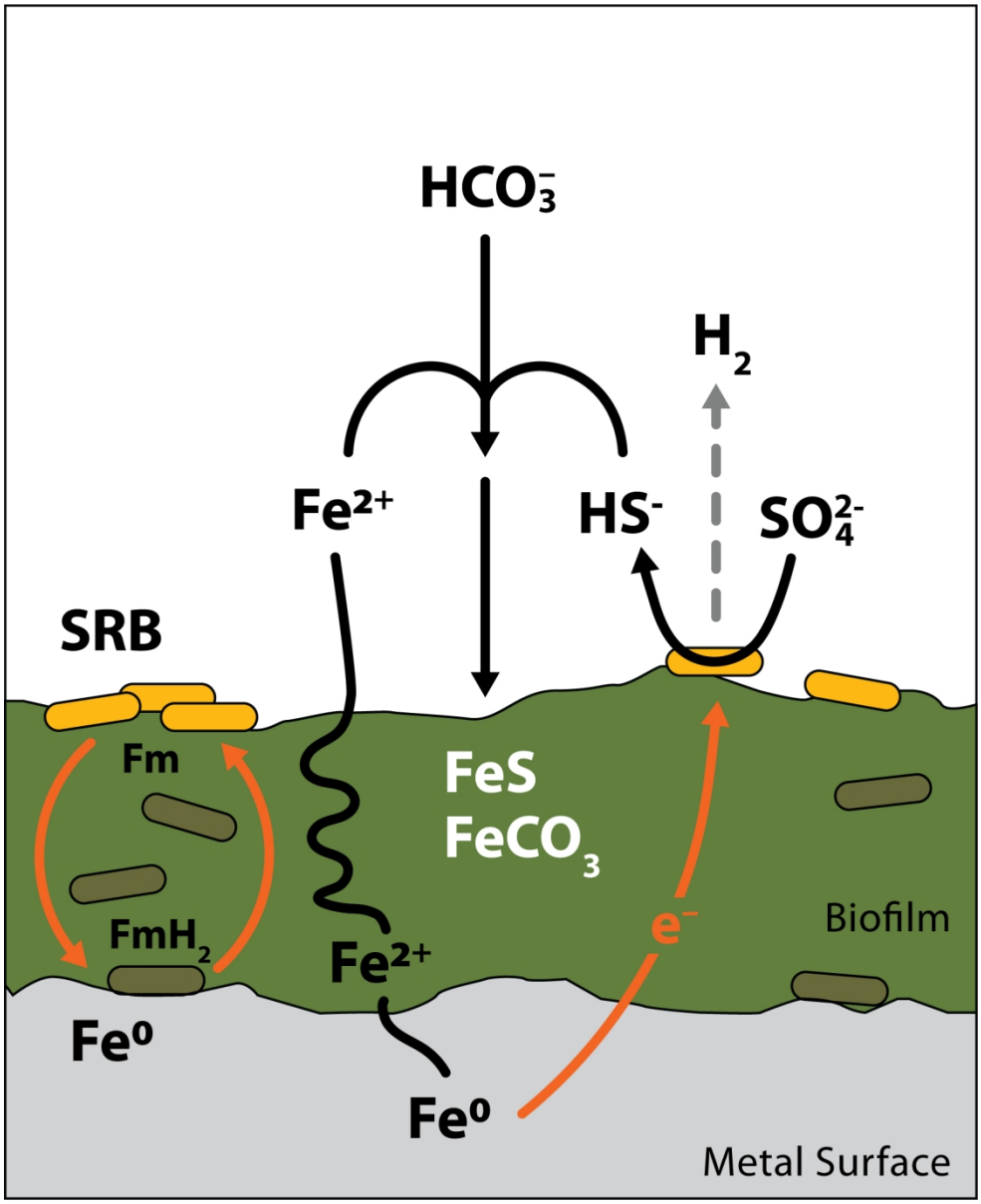

Figure 9. Classic model of corrosion with the addition of cycling endogenously produced flavin-based extracellular electron transfer molecules (Fm) with elemental Fe0 within the biofilm as a form of EET (extracellular electron transfer)-MIC. The dashed arrow to H2 could occur when electron acceptors (e.g., sulfates) are at low levels.

143x175mm (300 x 300 DPI)

Table 1. Planktonic growth yields (mg protein/M substrate or product) are shown from EAL (electron-acceptor limited), EDL (electron-donor limited), and 60:50 media calculated from sulfate consumption, lactate consumption, and acetate production.

	Sulfate Yield	**Lactate Yield**	**Acetate Yield**
EAL	0.042 ± 0.006	0.014 ± 0.002	0.033 ± 0.004
EDL	0.042 ± 0.008	0.032 ± 0.006	0.021 ± 0.004
60:50	0.025 ± 0.003	0.018 ± 0.002	0.027 ± 0.003

Table 2. Metabolites that differed significantly between EAL vs. EDL and have been confirmed with MS/MS.

Metabolite	Condition	Fold Change	p-value	q-value
Sulfolactate	Up in EAL	15.7	0.00003	0.0023
Cysteine-S-sulfate related	Up in EAL	20.1	0.0025	0.0122
Lumichrome	Up in EDL	10.1	0.0019	0.0019

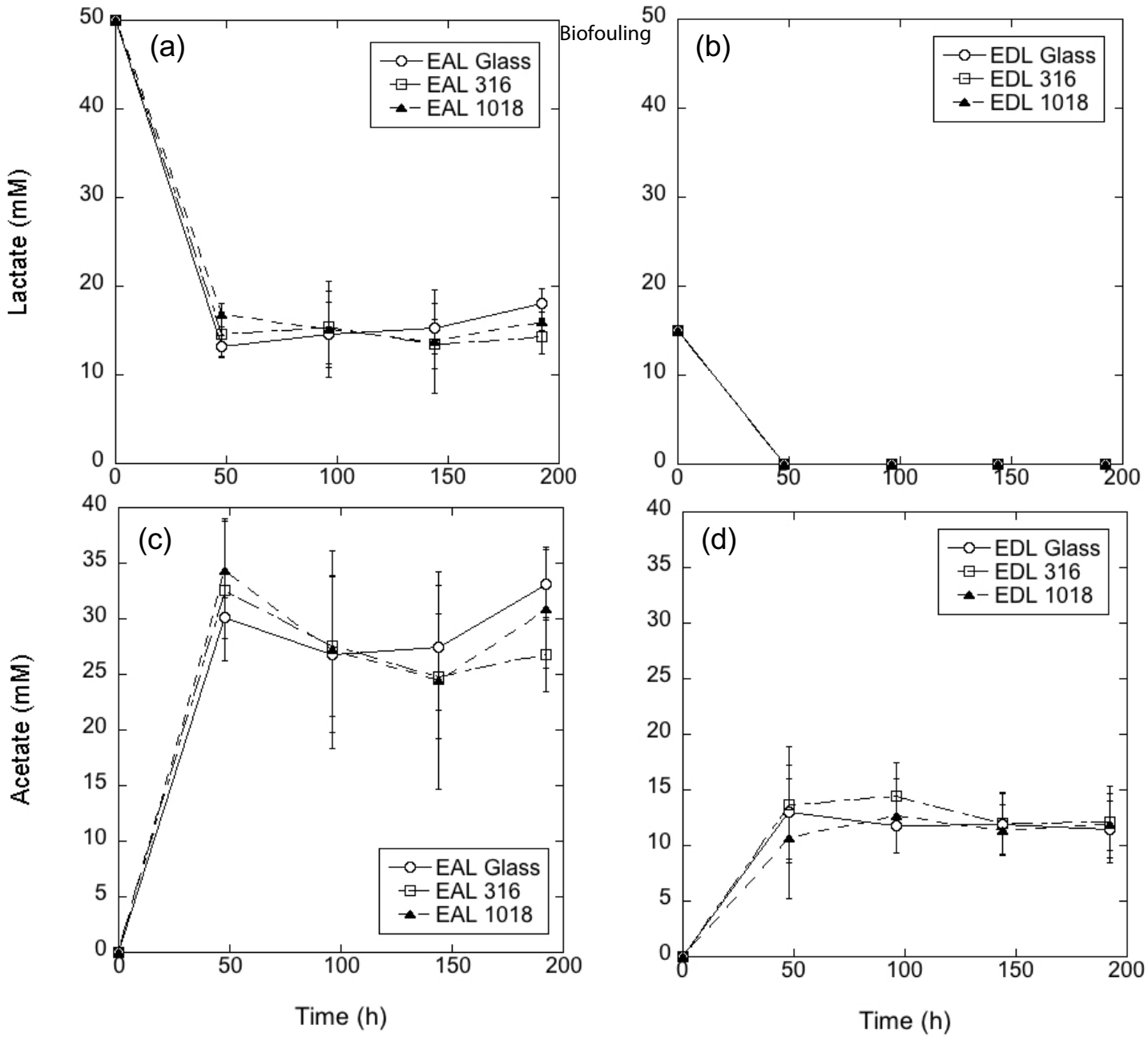

Figure S1. (a) Lactate levels are shown under EAL condition on glass, 316 stainless steel, and 1018 carbon steel surfaces; as well as (b) Lactate levels under EDL condition on all three surface types. (c) Acetate levels under EAL condition on all 3 surfaces are shown with (d) Acetate levels under EDL condition on all three surface types.

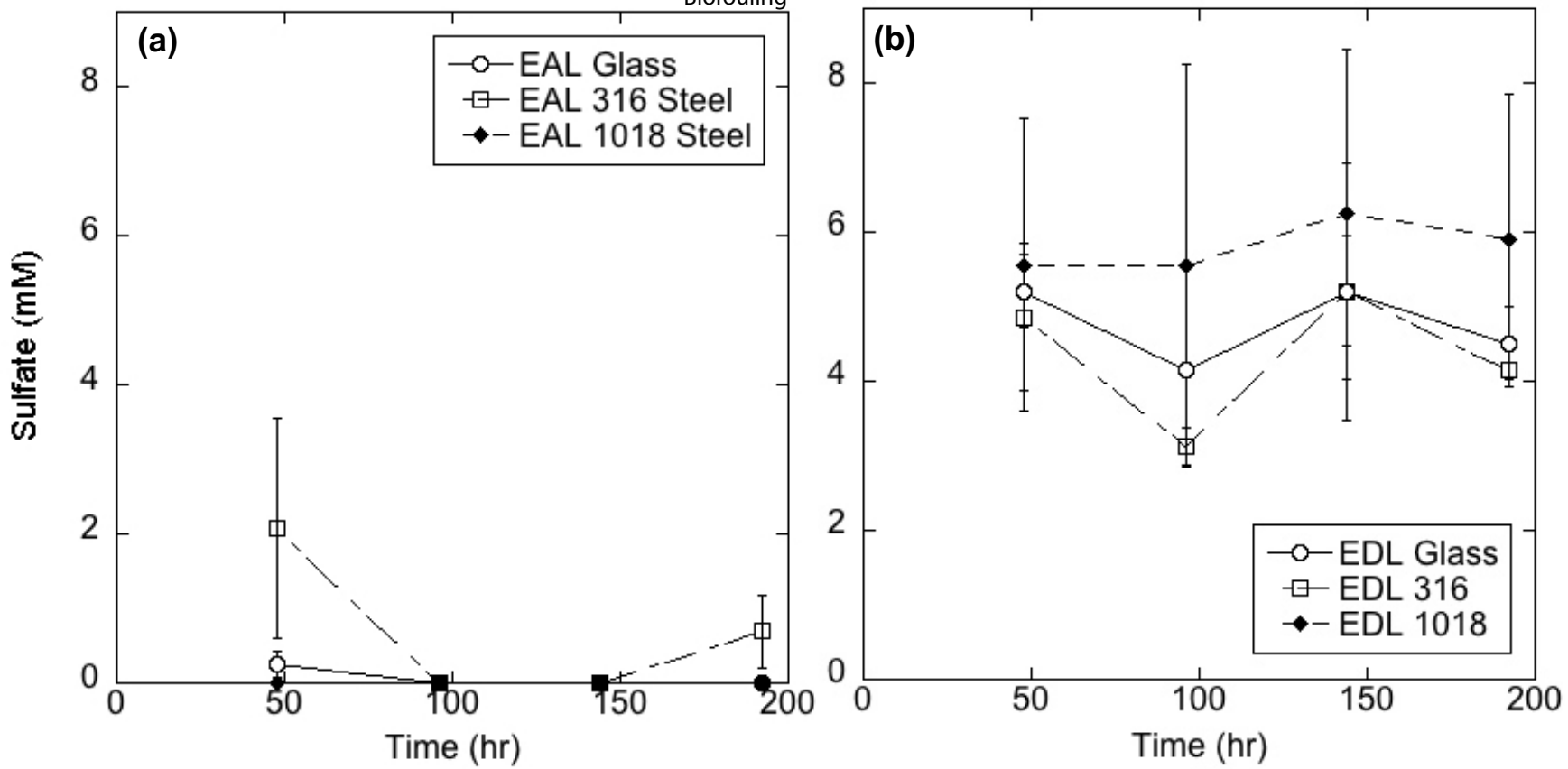

Figure S2. (a) Planktonic sulfate concentrations under EAL conditions. (b) Planktonic sulfate concentrations under EDL conditions.

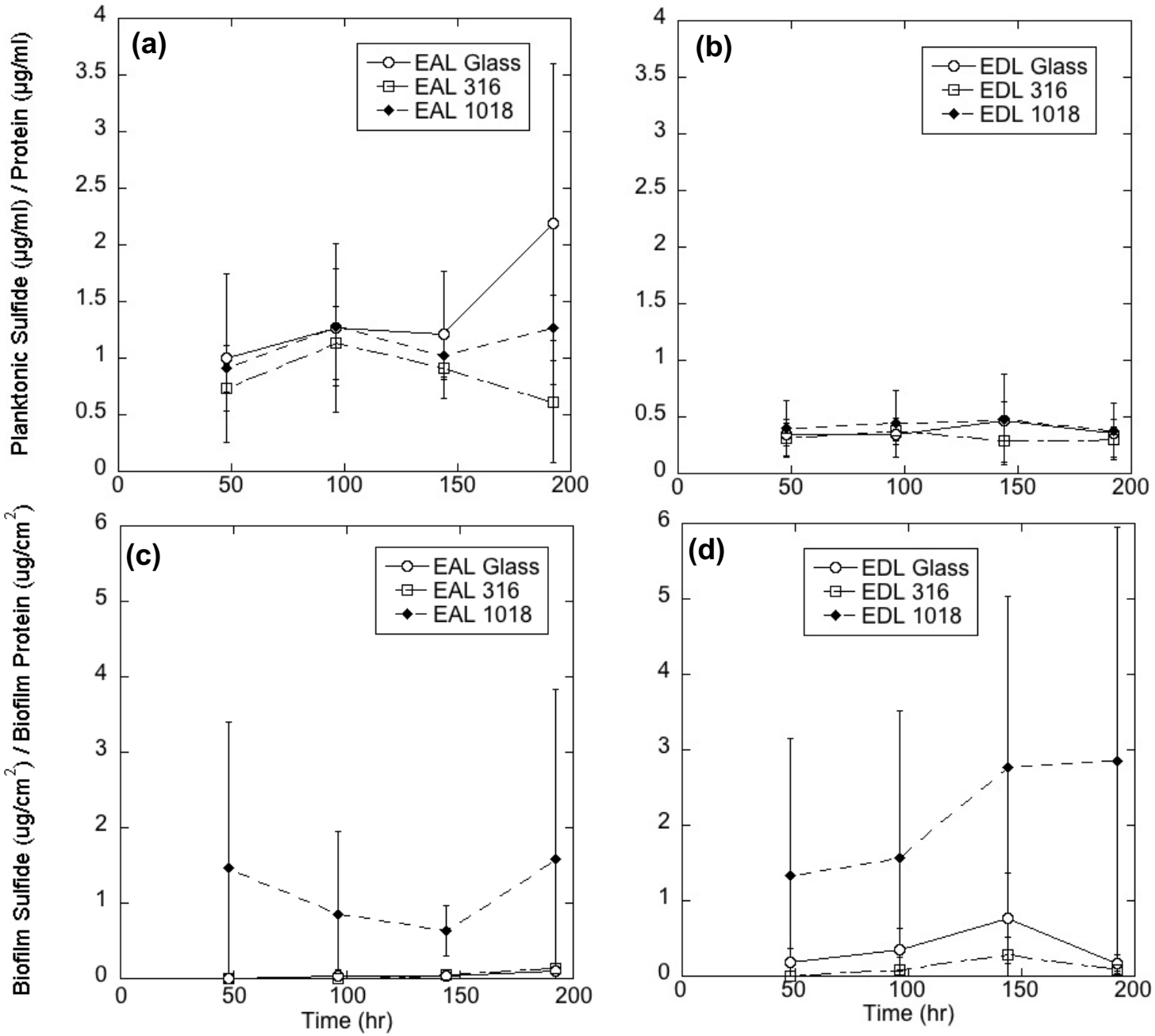

Figure S3. Sulfide was measured and normalized to protein levels. Biofilm sulfide levels were also normalized to surface area. (a) Planktonic sulfide concentrations under EAL conditions. (b) Planktonic sulfide levels under EDL conditions. (c) Biofilm sulfide levels under EAL conditions. (d) Biofilm sulfide levels under EDL conditions.